Reconfigurable Elastic Metamaterials: Engineering Dispersion with Beyond Nearest Neighbors

G.J. Chaplain⬤,* I.R. Hooper, A.P. Hibbins, and T.A. Starkey⬤
Centre for Metamaterial Research and Innovation, Department of Physics and Astronomy, University of Exeter, Exeter EX4 4QL, United Kingdom

We design, simulate, and experimentally characterize a reconfigurable elastic metamaterial with beyond-nearest-neighbor (BNN) coupling. The structure is composed from the popular British model-construction system Meccano and supports backward waves with opposite directions of phase and group velocities. We experimentally verify three distinct configurations and acoustically infer their spatial vibration spectra.

I. INTRODUCTION

Dispersive waves, the velocity of which varies nonlinearly with frequency, are of great interest to the wave-physics community. Metamaterials are structured materials with often periodic structuring that are capable of supporting such waves, which owe their dispersive properties due to their geometric design. Metamaterial concepts were originally explored in the electromagnetic domain [1–4], but quickly saw the ideas translated to other wave systems, from acoustics to elasticity [5–8], and to other periodic systems such as photonic and phononic crystals [9,10]. The engineering of dispersive wave properties is of particular importance in mechanical systems where vibration isolation and energy-harvesting devices rest on manipulating elastic wave propagation; elastic metamaterials offer the promise to unlock such applications. Such devices span orders of magnitude in length scale, from microscale surface-acoustic-wave (SAW) devices [11] and mesoscale bench-top devices [12,13] all the way up to macroscale seismic metamaterials [14,15] for ground-borne vibration control. Backward waves are one class of dispersive waves that possess unique properties; their phase and group velocities are antiparallel and as such the propagation of wave fronts is in the opposite direction to the energy flow—a phenomenon well known to electrical engineers since the early 1960s [16] and that occurs naturally in certain settings in elasticity, such as for Lamb modes in anisotropic plates and axisymmetric modes in pipes

[17–20], where their applications include the scattering and focusing of sound [21,22]. Recent advances in elastic and acoustic metamaterials [23] have achieved analogous backward-wave effects that can be bespoke and dictated by their structure, offering a route to tailoring dispersion by introducing reconfigurable components.

Metamaterial design and functional interpretation is often predicated on the analysis of wave propagation in periodic structures [24,25]. The ubiquity of such systems has inspired similar analytical techniques to be adopted to describe wave phenomena varying from the crystal scattering of x rays, to thermal vibrations in crystal lattices, to electron motion in metals, and to analogous electrical-engineering systems such as electromagnetic wave propagation in periodic circuits [26, 27]. Indeed, this analysis can be traced back to the "delightfully written" [28] seminal work of Léon Brillouin [26], who devotes a mathematical treatment to wave propagation in periodic structures, founded on a simple coupled-resonator model in the form of particles coupled by elastic springs. The introduction of Brillouin zones (BZs) and their relation to the reciprocal lattice forms the foundation for interpreting the dispersion, i.e., the frequency–wave-vector relation $\omega(\mathbf{k})$, of waves supported within periodic structures; the overarching theme connecting the disparate areas of physics described by this theory is that the associated periodic boundary conditions are satisfied by Bloch-Floquet waves that provide elegant solutions in the framework that the reciprocal lattice and associated irreducible Brillouin zone (IBZ) provide.

The canonical introductory model for periodic structures is a mechanical one-dimensional infinite chain of identical masses coupled to nearest neighbors (NNs) by identical springs. This is now commonplace in undergraduate courses and, indeed, is the starting model of Brillouin

---

*g.j.chaplain@exeter.ac.uk

[26]. This exemplar system exhibits a nonlinear dispersion relation, a cutoff frequency for systems of equal particles, and pass and stop bands for systems of different particles. The dispersion relation can be altered by including BNN coupling; as discussed by Brillouin, for interactions extending to the Lth nearest neighbor, the form of the dispersion relation [26]

"$[\cdots]$ will be expressed as a polynomial of degree L."

And so, as described by Brillouin, for interactions with the Lth nearest neighbor, there will be $L-1$ extrema within the first Brillouin zone, resulting in regions with altering signs of the group velocity, $\mathbf{v}_g = \partial\omega/\partial\mathbf{k}$. For the case of NN-only interactions, the singular extrema occurs at the band edge owing to the formation of standing waves via the Bragg condition.

BNN coupling is not unique to metamaterials or other periodic analogs. Indeed, it is commonplace to account for additional (sometimes "nonlocal") interactions when considering substantially more complex electronic band structures, where extra couplings arise in, e.g., tight-binding models [29,30], $\mathbf{k}\cdot\mathbf{p}$ perturbation theory [31], and density-functional theory [32,33].

A coalescence of the ideas surrounding BNN interactions has recently been realized for acoustic and elastic metamaterials and, specifically, next-next-nearest neighbors, i.e., $L=3$ [23,34], that have also been described as nonlocal metamaterials [35]. The intricately designed structures of Ref. [23] interconnect one unit cell with a physical join to one three unit cells away, providing an additional degree of interaction and an alternative channel for power flow. The maxima and minima of the modal dispersion within the first Brillouin zone are associated with these competing channels, resulting in a characteristic dispersion relation that shows some analogies to that of rotons [23].

Competing power channels, leading to regions of negative dispersion, can be achieved by other means than physically joined BNN coupling in acoustics and elasticity. Indeed, in electromagnetic metamaterials, such as the Sievenpiper "mushroom array" [36], there are no geometrical elements that couple beyond the fundamental cell but inherent competing power channels above (air) and below (hyperbolic media, vias) the structured surface result in regions of negative dispersion within the first Brillouin zone. Extensions of this are well documented in electromagnetism for both bulk and surface waves [37–41] and for waveguide modes [42]. Similar tailored dispersion relations can arise from other mechanisms, such as chiral induction in micropolar elastic materials [43], symmetry breaking [44,45] and topology [46,47].

In this paper, taking inspiration from the recent "roton-like" metamaterials, we design, simulate, and experimentally characterize a modular fully reconfigurable elastic metamaterial with beyond-nearest-neighbor coupling, compared to recent designs that are often fabricated via additive layer manufacturing (3D printing) [48]. We overcome the "serious experimental challenge" [49] surrounding the decoupling of NN and BNN connections by designing an elastic metamaterial that is easily reconfigurable using the popular British model-construction kit Meccano™, owing to its modular cost-effective design (and partly due to childhood nostalgia). For over a century, Meccano™ has been the first opportunity for aspiring young scientists and engineers to explore aspects of mechanics by designing, building, and playing with the sets, which typically contain building blocks such as strips, plates, and angle girders, with additional components such as wheels, axles, and gears. We opt to design in the earlier-style steel product, rather than the modern-day plastic equivalent, due to its elastic material properties. As such, the dimensions are quoted in imperial units (inches) as in the original designs [50]. We leverage the structure to investigate multiple modes with a potentially arbitrary number of extrema within the first BZ and, crucially, use the reconfigurable nature of the metamaterial to manipulate degeneracies in the band structure by breaking geometrical symmetries. The experimental characterization of the structure is unique in that we measure the acoustic pressure fluctuations as opposed to direct measurements of the elastic fields via expensive laser Doppler velicometry (LDV).

II. RECONFIGURABLE METAMATERIALS: DESIGN

In order to facilitate physical intuition about the expected modal behavior of an elastic metamaterial with BNN coupling, based upon Meccano™, we turn to a canonical mass-spring toy model, akin to Brillouin [26]. The toy model is composed of two coupled chains of dipolelike masses, linked to nearest neighbors by springs, with additional BNN coupling to the third-nearest neighbor, a schematic of which is shown in Fig. 1(c). The two supported modes have $L-1=2$ extrema within the first BZ, forming a pair of orthogonal modes as shown in Fig. 1(b). Figure S1 in the Supplemental Material [52] details the masses and spring constants used to formulate the governing difference equation and the ensuing eigenvalue problem. The toy mass-spring model allows intuition to be gained on the influence of symmetry breaking on the dispersion relations of the modes supported by the chains, which we investigate through our proposed reconfigurable structure. We are concerned with the lowest two bending modes of the structure, where the displacement is predominantly out of the plane and where the ends of the beam oscillate either in phase or out of phase, as shown by the even and odd eigenmodes, respectively, in Fig. 2(b). In the toy model, we constrain the displacements of the masses to also only be in one direction (x), such that the
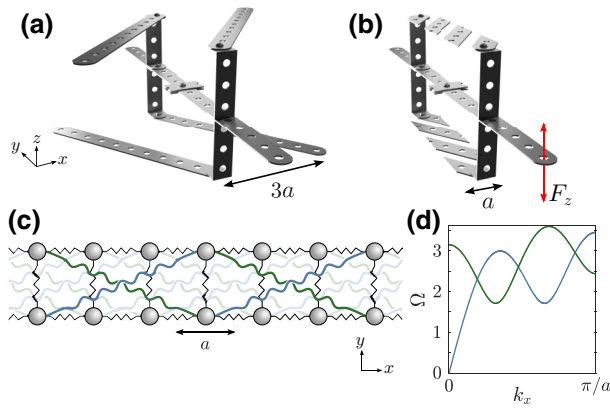
FIG. 1. Example Meccano geometry and corresponding toy model. (a) The unit cell with BNN connections, with (b) showing the periodically repeating unit cell of width a. The red arros shows the possible applied force, F_z, to excite bending modes of the structure. (c) Schematic of toy mass-spring model with BNN coupling (green and blue springs), with (d) the corresponding dispersion curves with multiple extrema within the first BZ.

chains of masses can oscillate either in phase or out of phase in an analogous fashion to the beams. A limitation of this is that the toy model does not recover the acoustic-acoustic phonon behavior of the lowest two modes: Only the lowest band approaches zero frequency as $k_x \to 0$ [e.g., Fig. 2(b)]. Instead, the branches in the toy model display classical acoustic-optical bands that are conventional with, e.g., a two-mass unit cell [26]. The optical branch corresponds to the phase difference of the mass chains, resulting in the center of mass remaining at rest, which occurs with finite nonzero frequency at $k = 0$. The introduction of phase-velocity limiting terms associated with the bulk compressional and transverse wave speeds, as in Ref. [24], can constrain the mass-spring chains so that similar acoustic-acoustic branches exist—for simplicity, we do not consider this here. In Fig. 1(a), we highlight the unit cell of one of the possible configurations of the metamaterial, resulting from an extension of the toy model.

Our designs are built from cold-rolled steel (see Sec. III) and comprise two key components to introduce coupling on different length scales within the structure: (1) a central strip that runs the length of the sample, to which perpendicular beams are attached, and (2) inter-unit-cell connecting strips that form a scaffold above and below the central strip, making use of a convenient Pythagorean triple that fits the discrete holes available on the original Meccano™ designs, each spaced by 0.5 in. The central beam provides nearest-neighbor coupling between unit cells (of width a), of which the perpendicular arms are the main resonant element, and the connectors provide BNN coupling. This design can be interpreted using the toy model: the perpendicular arms and angled joints to the connectors approximate lumped masses connected by the

vertical springs in the toy model. The central beam forms the springlike connection to adjacent cells in each chain of masses, with the connectors providing the analogy to the long-range springs as shown in Fig. 1(c). The lowest two bending modes of the perpendicular arms, where the displacement is predominantly in the z direction, then possess the same symmetries as the two eigenmodes present in the toy model.

The structure can be configured in a number of ways to tailor the mode dispersion. We demonstrate three configurations, which are easily built and rebuilt, and support modes with distinct dispersive characteristics. We obtain the dispersion curves for each configuration using the finite-element method (FEM) [51], solving the 3D equations of elastodynamics in the frequency domain. We define two of the three configurations in relation to the symmetry of the perpendicular arm with respect to the $z - x$ plane through the central beam and term them as follows: (i) the symmetric configuration [Fig. 2(a)], where the perpendicular arm extends symmetrically in y from the central beam and the connectors above and below the central beam are crossed; (ii) the asymmetric configuration [Fig. 2(c)], where the perpendicular arm is displaced so that the arm is longer on one side of the connectors (and therefore asymmetric about the central beam); and (iii) a configuration that returns to a symmetric arrangement of the perpendicular arm but now with the connectors above and below the central beam being parallel. A schematic of all parts is shown in Figs. 3(a) and 3(b), detailing the conventional imperial units of classic British Meccano™. The central beam section (component 1) is periodically repeated along the axis of the sample, in the x direction.

The lowest eigenfrequencies of each configuration are evaluated by employing Floquet-Bloch periodic boundary conditions in the FEM model and solving the ensuing eigenvalue problem. The periodic boundaries are highlighted as red edges in Fig. 2(a). Figures 2(b), 2(d), and 2(f) show the corresponding dispersion curves for the three configurations (i), (ii), and (iii), respectively. The color scale in each dispersion diagram represents the normalized integrated complex mechanical energy flux, $\mathbf{I} = -\boldsymbol{\sigma} \cdot \mathbf{v}^*$, where $\boldsymbol{\sigma}$ is the stress tensor and $\mathbf{v}^*$ is the complex conjugate of the velocity (in the direction of periodicity, I_x) over two regions: the left half of the dispersion curves shows the integrated complex mechanical energy flux over the connectors, as highlighted in magenta in Fig. 2(f), while the right half shows the same calculation over the perpendicular arms, as highlighted in green in Fig. 2(f). This quantity provides a relative measure of the power flow along the different channels provided by the short- and long-range couplings that co- and counterpropagate, demonstrating that it is these competing power flows that result in the extrema in the dispersion curves. Of course, the net power flow must always be away from a given source; in Fig. S3 in the Supplemental Material [52], we show the normalized
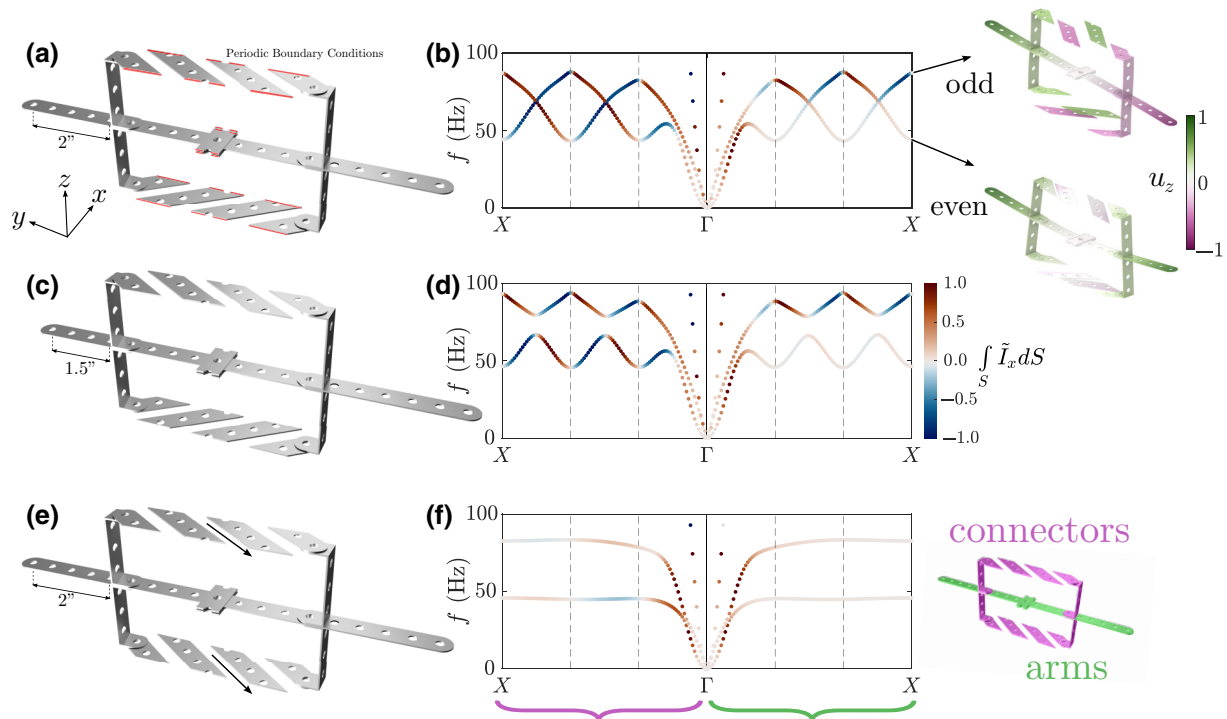
FIG. 2. The three unit-cell configurations and their respective dispersion curves. (a) A schematic of the unit cell for the symmetric configuration, with edges highlighted in red where periodic boundary conditions are employed in FEM modeling [51]. (b) Dispersion curves obtained via frequency-domain eigenvalue simulations. The color scale depicts the value of the normalized integrated mechanical energy flux in the direction of the periodicity, $\int_S \tilde{I}_x dS$, over the regions S that denote either the connectors (left-hand side of dispersion plot) or the arms (right-hand side of dispersion plot). At the band edge, the eigenmode shapes are shown, with the color scale showing the normalized out-of-plane displacement, u_z; the displacement of the perpendicular arm is purely odd or even in z. The dashed lines indicate $k_x = \pm\pi/3a$ and $k_x = \pm 2\pi/3a$. (c),(e) The schematics of the unit cells for the asymmetric and parallel configurations, respectively, with the asymmetric length of the arms in (c) highlighted and the parallel nature of the connectors highlighted in (e). (d),(f) Dispersion curves, as in (b), but for the asymmetric and parallel configurations, respectively. Shown next to (f) is a schematic of the regions S (the connectors and arms) over which the complex mechanical energy flux is integrated.

sum of the complex mechanical energy fluxes over the two channels (arms and connectors), confirming that the sign of the net power follows that dictated by the sign of the gradient of the dispersion curves.

Each of the three configurations possesses unique dispersive properties that are related to the internal symmetries possessed by the unit cell. As we consider the lowest two bending eigenmodes, we describe the modal symmetries in terms of the out-of-plane displacement (u_z) of the perpendicular arms. In the symmetric configuration, the structure supports an orthogonal pair of eigenmodes [53] that manifest in the form of degeneracies in the band structure, i.e., at the points where the dispersion curves of the two modes cross. The out-of-plane displacement of the perpendicular arm is (anti)symmetric, giving rise to the notion of (odd)even modes, as shown by the out-of-plane displacement fields in Fig. 2(b) at the band edge where the wave vector $k_x = X \equiv \pi/a$; standing waves form here and the energy flux along the structure vanishes.

The orthogonality of these modes suggests they can be excited independently or mixed by utilizing a forcing that matches the modal symmetry (see Sec. IV).

The asymmetric configuration breaks the reflectional symmetry of the perpendicular arm about the z-x plane defined through the central beam, thereby lifting the degeneracies present in the dispersion curves for the symmetric configuration. This is shown in Fig. 2(d), where the mixing of the modes can be seen when comparing the energy fluxes of the symmetric and antisymmetric modes along the arms, resulting in anticrossings between the positively and negatively dispersing modes. We show the eigenmode shapes where the out-of-plane displacement of the perpendicular arm is neither odd nor even in Fig. S3 in the Supplemental Material [52].

In the parallel configuration, the perpendicular arms are once again symmetric about the z-x plane defined through the central beam but rotational symmetry about the y axis is broken. The resulting dispersion curves are much

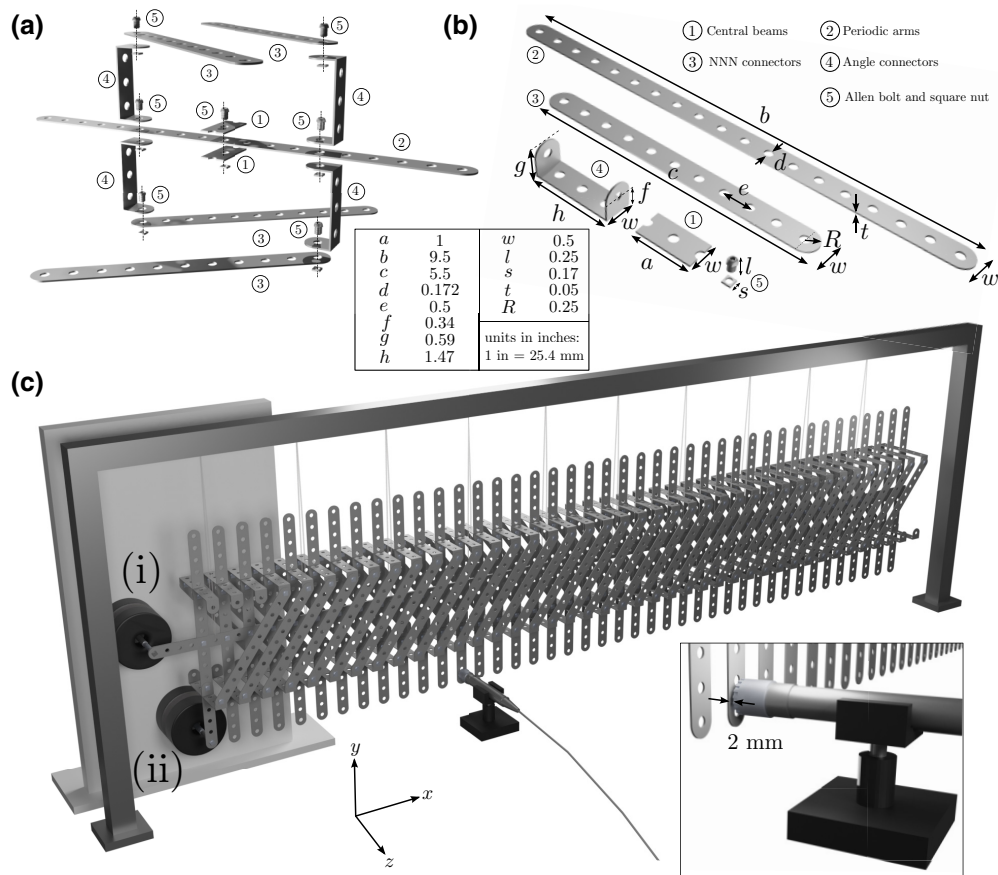| a	1	w	0.5
b	9.5	l	0.25
c	5.5	s	0.17
d	0.172	t	0.05
e	0.5	R	0.25
f	0.34	units in inches:
g	0.59	1 in = 25.4 mm
h	1.47	

FIG. 3. Schematic diagrams. (a) An instruction-manual-style diagram for constructing the unit cell (symmetric configuration example). (b) The Meccano™ pieces required for the unit cell. Note that the central beam shown is periodically repeated and forms a whole beam for the entire length of the structure. (c) The experimental setup for acoustically characterizing the dispersion curves of the structure (full details are given in Sec. III).

flatter, although still retaining the same number of extrema within the IBZ. This orientation of connectors biases the direction of power flow along them, as seen by the integrated mechanical energy fluxes of the two channels, which remain predominantly aligned.

Having demonstrated the reconfigurable nature of the unit cells and the effects they have on the dispersion of the supported waves on an infinitely repeating system, we now present the experimental characterization of each configuration and compare with FEM simulations of the finite structure.

III. MATERIALS AND METHODS

A. Meccano™ components

A Meccano™ set is designed following the original dimensions set out in the "Liverpool" engineering drawings [50]. The components are laser cut by Luffman Engineering (Tiverton, UK), from a single 1.2-mm-thick mild-steel sheet [cold rolled (CR4)].

The sample is assembled, as shown in the manual-style schematic in Fig. 3(a), with original Meccano™ bolts [37b Allen bolt, 1/4 in. (6 mm), zinc] and corresponding square nuts.

B. Experimental setup and method

A schematic of the experimental setup is shown in Fig. 3(c). The sample is hung horizontally from a bar using nylon fishing wire, looped through the central strip that runs the length of the sample. The sample is excited using a mechanical shaker (PASCO Mechanical Wave Driver model no. 2185) driven by a variable-frequency signal generator (Agilent 33220A arbitrary waveform generator). Two excitation positions, (i) and (ii), [Fig. 3(c)] are considered, to provide either a symmetric displacement excitation [in (i)] or a displacement with mixed symmetry [in (ii)] in order to demonstrate the orthogonal nature of the modes in the symmetric configuration. For all measurements, the shaker is driven by a ±5 V peak-to-peak sine wave.

To measure the displacement of the vertical beams, the local pressure fluctuations in the air at each vibrating
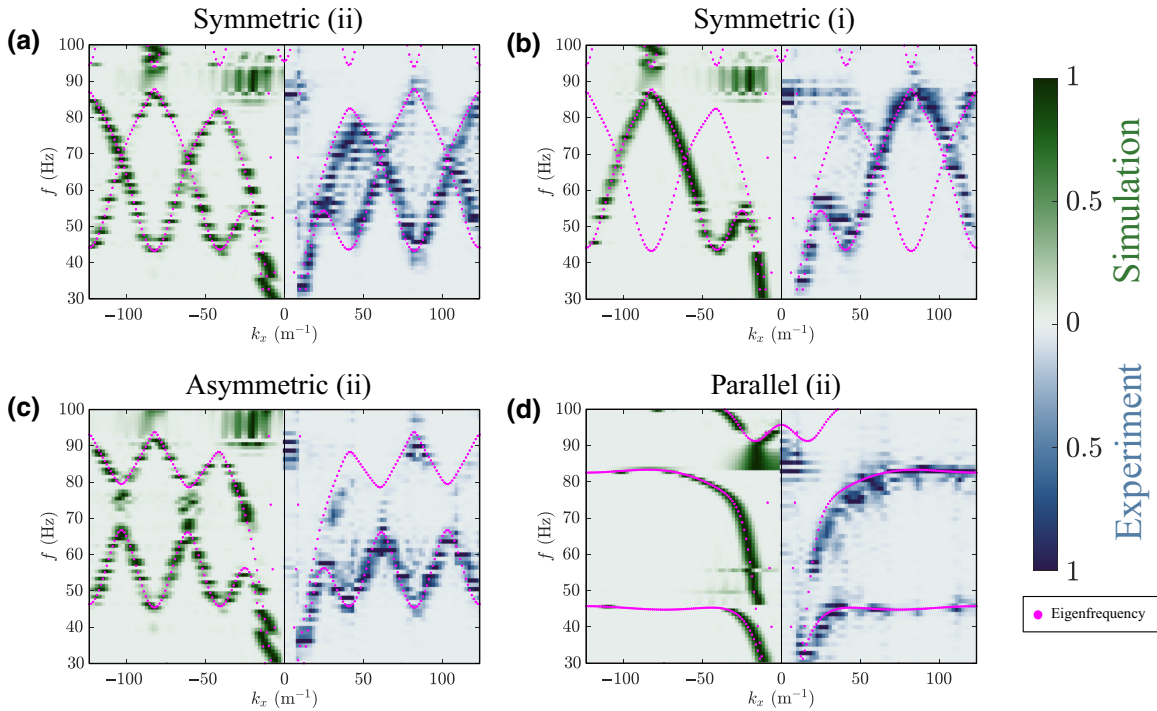
FIG. 4. Comparisons between the numerical (FEM) and experimental results. (a) The normalized, per frequency, Fourier amplitude of the numerically (left-hand side) and experimentally (right-hand side) determined dispersion spectra, for the symmetric configuration excited in position (ii) from 30 to 100 Hz in 1-Hz steps. Overlaid are the eigenfrequency solutions from the infinitely periodic model (Fig. 2). (b) As for (a) but for excitation in position (i), therefore isolating the even mode. (c) As for (a) but for the asymmetric configuration. (d) As for (a) but for the parallel configuration.

arm are recorded. At each arm, a microphone (Brüel & Kjær Type 4940 1/2-in. free-field microphone, with a preconditioning amplifier) is positioned 2 mm from the sample, so that the head is centered in the width of the Meccano™ bar horizontally and between the two lower holes vertically (as shown in Fig. 3(c), inset) and the signal is recorded on an oscilloscope (Siglent SDS2352X-E). The acoustic data are recorded with a sampling frequency of 500 kSa s^{-1} for a total time of 0.28 s and with 16 averages.

The experimental procedure is as follows: the microphone is positioned at the first arm, the structure is driven to a steady state at discrete frequencies (30–100 Hz in 1-Hz steps), and the signal from the is microphone recorded. This is repeated at each arm.

To determine the mode dispersion, the temporal acoustic signals are summed at each arm, producing a signal (voltage) as a function of the propagation distance and time $V(x, t)$. The data are processed using temporal and spatial Fourier transformation with a Tukey window function applied to determine the wave-number–frequency relation.

C. Numerical simulations

The dispersion curves (Fig. 2) of each configuration are obtained via the FEM model using an eigenfrequency study in the Solid Mechanics module within COMSOL

MULTIPHYSICS (version 6.0), with Floquet-Bloch boundary conditions applied as shown in Fig. 2(a). Example eigenmodes (and the unit cell) are shown in Fig. S3 in the Supplemental Material [52]. The dispersion spectra shown in Fig. 4 is obtained through a frequency-domain simulation of 41 unit cells of the metamaterial (*in vacuo*) with free boundary conditions on all boundaries except the position of the shaker, which is modeled as a boundary load at positions (i) and (ii), as in Fig. 3(c). The simulations are performed with the boundary load driven at the same set of discrete frequencies as used in the physical experiment (30–100 Hz in 1-Hz steps). The out-of-plane displacement is then extracted along a line down the length of the sample and analyzed by means of the spatial FFT. A schematic of the computational domain and boundary conditions is shown in Fig. S4 in the Supplemental Material [52]. The mild-steel mechanical material properties of the Meccano™ are assumed to be density $\rho = 7870$ kg/m^3, Poisson's ratio $\sigma = 0.287$, and elastic modulus $Y = 210$ GPa.

IV. RESULTS

Owing to the scarcity of original pieces and the variations in its composition and material properties, a

custom-made Meccano™-like set is fabricated following the original dimensions [50], and assembled into the unit cells following the schematic in Fig. 3(a). Figure 3(c) shows the full structure, in the symmetric configuration, consisting of 41 unit cells, with an extended central beam to which the shaker is attached at either position (i) or (ii), depending on the desired excitation condition. The structure is suspended from a rigid frame using nylon wire at equally spaced points along the beam length [as shown in Fig. 3(c)]. We adopt a simple experimental setup to measure the vibrations acoustically. The local pressure fluctuations in the air generated by the vibrating arms are measured by the microphone and the dispersion spectra recovered by spatiotemporal Fourier analysis of the data by means of the fast Fourier transform (FFT). The experimental results are shown in Fig. 4 on the right-hand side of each plot; the left-hand side of each plot shows the results from frequency-domain FEM simulations that mirror each of the experimental configurations: the same finite number of unit cells are simulated with corresponding forcing conditions at the shaker positions and the out-of-plane displacement is extracted along the perpendicular arms and analyzed by a spatial FFT to obtain the dispersion spectra along the structure, as shown in Fig. S4 in the Supplemental Material [52].

Figure 4 shows the excellent agreement between the numerically simulated and experimental dispersion curves, normalized on a per-frequency basis. Figure 4(a) shows comparisons of the numerical and experimental dispersion for the symmetric configuration excited in position (ii), as shown in Fig. 3(c), which contains a mixture of the even and odd modes shown in Fig. 2(b). Figure 4(b) shows a similar comparison but for excitation at position (i); this only drives modes with an even out-of-plane displacement of the perpendicular arms, as the source is aligned with the propagation axis. Figures 4(c) and 4(d) show the comparisons for the asymmetric and parallel configurations, respectively. In all four plots, the eigenfrequency results for the infinitely periodic case are overlaid (Fig. 2). For the case of the asymmetric configuration [Fig. 2(c)], the shaker and measurement position are on the longer side of the asymmetric perpendicular arm (Fig. S4 in the Supplemental Material [52]).

V. DISCUSSION

The dispersion characteristics of elastic metamaterials and other periodic structures are conventionally fixed once the sample has been fabricated. Here, we develop a reconfigurable elastic metamaterial that leverages beyond-nearest-neighbor interactions, capable of supporting backward waves. Qualitative analogies to a canonical mass-spring model motivate the design paradigm surrounding the symmetries of the structure. The BNN coupling provides alternative channels for power flow, the

competition between which results in extrema within the first Brillouin zone and as such unlocks motivation for vibration-sensing applications in, e.g., scaled down SAW devices by structuring the SAW-carrying substrate, as in Ref. [15,54], rather than, say, the transducer array that generates them, as in Ref. [55]. Backward waves have found recent applications as liquid sensors [56] and therefore offer an alternative route to conventional capabilities of SAW devices such as acoustofluidics for sensing or mixing [57].

Further applications come in the form of elastic energy harvesters; graded elastic metamaterials [58,59] have been identified as attractive candidates for passive vibrational energy harvesting, where slow waves are used in conjunction with piezoelectric harvesters. These devices rely on leveraging zero-group-velocity modes and it has been shown that there is a distinction between zero-group-velocity modes that exist within the first BZ, due to competing power flows, and those that exist at the band edge by virtue of the Bragg condition, with the former being the more attractive candidates for harvesting applications [44]. These "rainbow-trapping" devices rely on symmetry-broken arrays of longitudinally vibrating rods on an elastic beam, which have recently been realized with flexurally vibrating harvesters [60], of which our structure is reminiscent. Due to the reconfigurable nature of our devices, grading can easily be incorporated and, as we show throughout, extrema in the band structure (and hence the existence of multiple zero-group-velocity modes) are straightforward to design. As such, these structures, and extensions thereof, offer an attractive route to applications in elastic energy harvesting.

The device is inspired by the popular model-construction kit Meccano™ and motivates the development of analogous modular metamaterials with replaceable components in addition to serving as a tactile innovative pedagogical method for introducing beyond-nearest-neighbor interactions in metamaterials and phononic crystals. The acoustic experimental characterization of the structure, by measuring the local pressure fluctuations induced by the resonant elements of the structure, provides an alternative method for vibration characterization on the laboratory-bench scale using simple acoustic methods, where more complex and expensive methods (e.g., LDV) may not be available.

The research data supporting this publication are openly available from the University of Exeter's institutional repository [61].

---

[1] V. G. Veselago, Electrodynamics of substances with simultaneously negative ϵ and μ, Usp. fiz. Nauk **92,** 517 (1967).

[2] J. B. Pendry, A. J. Holden, D. J. Robbins, and W. Stewart, Magnetism from conductors and enhanced nonlinear phenomena, IEEE Trans. Microw. Theory Tech. **47,** 2075 (1999).

[3] J. B. Pendry, Negative Refraction Makes a Perfect Lens, Phys. Rev. Lett. **85,** 3966 (2000).

[4] D. R. Smith, W. J. Padilla, D. C. Vier, S. C. Nemat-Nasser, and S. Schultz, Composite Medium with Simultaneously Negative Permeability and Permittivity, Phys. Rev. Lett. **84,** 4184 (2000).

[5] R. V. Craster and S. Guenneau, *Acoustic Metamaterials: Negative Refraction, Imaging, Lensing and Cloaking* Vol. 166 (Springer Science & Business Media, Dordrecht, 2012).

[6] X. Zhou, X. Liu, and G. Hu, and Elastic metamaterials with local resonances: An overview, Theor. Appl. Mech. Lett. **2,** 041001 (2012).

[7] M. I. Hussein, M. J. Leamy, and M. Ruzzene, Dynamics of phononic materials and structures: Historical origins, recent progress, and future outlook, Appl. Mech. Rev. **66,** 040802 (2014).

[8] M. Kadic, G. W. Milton, M. van Hecke, and M. Wegener, 3D metamaterials, Nat. Rev. Phys. **1,** 198 (2019).

[9] C. Luo, S. G. Johnson, J. D. Joannopoulos, and J. B. Pendry, All-angle negative refraction without negative effective index, Phys. Rev. B **65,** 201104 (2002).

[10] S. Foteinopoulou and C. M. Soukoulis, Electromagnetic wave propagation in two-dimensional photonic crystals: A study of anomalous refractive effects, Phys. Rev. B **72,** 165112 (2005).

[11] H. Kähler, D. Platz, and S. Schmid, Surface acoustic wave coupling between micromechanical resonators, Commun. Phys. **5,** 1 (2022).

[12] A. Colombi, V. Ageeva, R. J. Smith, A. Clare, R. Patel, M. Clark, D. Colquitt, P. Roux, S. Guenneau, and R. V. Craster, Enhanced sensing and conversion of ultrasonic Rayleigh waves by elastic metasurfaces, Sci. Rep. **7,** 1 (2017).

[13] G. J. Chaplain, J. M. De Ponti, G. Aguzzi, A. Colombi, and R. V. Craster, Topological Rainbow Trapping for Elastic Energy Harvesting in Graded Su-Schrieffer-Heeger Systems, Phys. Rev. Appl. **14,** 054035 (2020).

[14] A. Colombi, D. Colquitt, P. Roux, S. Guenneau, and R. V. Craster, A seismic metamaterial: The resonant metawedge, Sci. Rep. **6,** 1 (2016).

[15] C. Pouya and G. R. Nash, Sub- and supersonic elastic waves in an annular hole phononic metamaterial, Commun. Mater. **2,** 1 (2021).

[16] P. Clarricoats and R. Waldron, Non-periodic slow-wave and backward-wave structures, Int. J. Electron. **8,** 455 (1960).

[17] R. Mindlin, in *11th Annual Symposium on Frequency Control* (IEEE, 1957), p. 1.

[18] A. Shuvalov and O. Poncelet, On the backward Lamb waves near thickness resonances in anisotropic plates, Int. J. Solids Struct. **45,** 3430 (2008).

[19] K. Tamm, T. Peets, J. Engelbrecht, and D. Kartofelev, Negative group velocity in solids, Wave Motion **71,** 127 (2017).

[20] C. Chapman and S. Sorokin, A Wronskian method for elastic waves propagating along a tube, Proc. R. Soc. A **477,** 20210202 (2021).

[21] P. L. Marston, Negative group velocity Lamb waves on plates and applications to the scattering of sound by shells, J. Acoust. Soc. Am. **113,** 2659 (2003).

[22] T. J. Graham, J. D. Smith, A. P. Hibbins, J. R. Sambles, and T. A. Starkey, Experimental characterization of acoustic beaming from an elastic plate by coupled symmetric leaky Lamb modes, Phys. Rev. B **104,** 045105 (2021).

[23] Y. Chen, M. Kadic, and M. Wegener, Roton-like acoustical dispersion relations in 3D metamaterials, Nat. Commun. **12,** 1 (2021).

[24] A. A. Maznev and V. E. Gusev, Waveguiding by a locally resonant metasurface, Phys. Rev. B **92,** 115422 (2015).

[25] K. H. Matlack, M. Serra-Garcia, A. Palermo, S. D. Huber, and C. Daraio, Designing perturbative metamaterials from discrete models, Nat. Mater. **17,** 323 (2018).

[26] L. Brillouin, *Wave Propagation in Periodic Structures: Electric Filters and Crystal Lattices* (Dover, New York, 1953), 2nd ed..

[27] G. V. Eleftheriades, A. K. Iyer, and P. C. Kremer, Planar negative refractive index media using periodically *L-C* loaded transmission lines, IEEE Trans. Microw. Theory Tech. **50,** 2702 (2002).

[28] M. Born, Wave propagation in periodic structures, Nature **158,** 926 (1946).

[29] A. Hill, S. A. Mikhailov, and K. Ziegler, Dielectric function and plasmons in graphene, EPL (Europhys. Lett.) **87,** 27005 (2009).

[30] A. H. Castro Neto, F. Guinea, N. M. R. Peres, K. S. Novoselov, and A. K. Geim, The electronic properties of graphene, Rev. Mod. Phys. **81,** 109 (2009).

[31] J. M. Luttinger and W. Kohn, Motion of electrons and holes in perturbed periodic fields, Phys. Rev. **97,** 869 (1955).

[32] P. Hohenberg and W. Kohn, Inhomogeneous electron gas, Phys. Rev. **136,** B864 (1964).

[33] W. Kohn and L. J. Sham, Self-consistent equations including exchange and correlation effects, Phys. Rev. **140,** A1133 (1965).

[34] J. A. Iglesias Martínez, M. F. Groß, Y. Chen, T. Frenzel, V. Laude, M. Kadic, and M. Wegener, Experimental observation of roton-like dispersion relations in metamaterials, Sci. Adv. **7,** eabm2189 (2021).

[35] K. Wang, Y. Chen, M. Kadic, C. Wang, and M. Wegener, Nonlocal interaction engineering of 2D roton-like

dispersion relations in acoustic and mechanical metamaterials, Commun. Mater. **3**, 1 (2022).

[36] D. Sievenpiper, L. Zhang, R. F. Broas, N. G. Alexopolous, and E. Yablonovitch, High-impedance electromagnetic surfaces with a forbidden frequency band, IEEE Trans. Microw. Theory Tech. **47**, 2059 (1999).

[37] H. Shin and S. Fan, All-Angle Negative Refraction for Surface Plasmon Waves Using a Metal-Dielectric-Metal Structure, Phys. Rev. Lett. **96**, 073907 (2006).

[38] H. J. Lezec, J. A. Dionne, and H. A. Atwater, Negative refraction at visible frequencies, Science **316**, 430 (2007).

[39] J. Yao, Z. Liu, Y. Liu, Y. Wang, C. Sun, G. Bartal, A. M. Stacy, and X. Zhang, Optical negative refraction in bulk metamaterials of nanowires, Science **321**, 930 (2008).

[40] J. A. Dockrey, S. A. R. Horsley, I. R. Hooper, J. R. Sambles, and A. P. Hibbins, Direct observation of negative-index microwave surface waves, Sci. Rep. **6**, 1 (2016).

[41] B. Tremain, I. R. Hooper, J. R. Sambles, and A. P. Hibbins, Isotropic backward waves supported by a spiral array metasurface, Sci. Rep. **8**, 1 (2018).

[42] S. S. Seetharaman, B. Tremain, W. L. Barnes, and I. R. Hooper, Realizing an ultra-wideband backward-wave metamaterial waveguide, Phys. Rev. B **98**, 235408 (2018).

[43] J. Kishine, A. S. Ovchinnikov, and A. A. Tereshchenko, Chirality-Induced Phonon Dispersion in a Noncentrosymmetric Micropolar Crystal, Phys. Rev. Lett. **125**, 245302 (2020).

[44] G. J. Chaplain, D. Pajer, J. M. De Ponti, and R. V. Craster, Delineating rainbow reflection and trapping with applications for energy harvesting, New J. Phys. **22**, 063024 (2020).

[45] G. P. Ward, J. D. Smith, A. P. Hibbins, J. R. Sambles, and T. A. Starkey, Gapless dispersion of acoustic line modes with glide symmetry, Phys. Rev. B **105**, 245401 (2022).

[46] B. G. Chen, N. Upadhyaya, and V. Vitelli, Nonlinear conduction via solitons in a topological mechanical insulator, Proc. Nat. Acad. Sci. **111**, 13004 (2014).

[47] L. Xin, Y. Siyuan, L. Harry, L. Minghui, and C. Yanfeng, Topological mechanical metamaterials: A brief review, Current Opin. Solid State Mater. Sci. **24**, 100853 (2020).

[48] D. B. Moore, J. R. Sambles, A. P. Hibbins, T. A. Starkey, and G. J. Chaplain, Acoustic surface modes on metasurfaces with embedded next-nearest neighbor coupling, arXiv e-prints, arXiv (2022).

[49] R. Fleury, Non-local oddities, Nat. Phys. **17**, 766 (2021).

[50] *Meccano Tech-Drawings (Liverpool drawings)* compiled by C. Clinchx, https://www.meccanoindex.co.uk/Drawings/Index.php (circa. 1939), accessed: 2022-05-17.

[51] COMSOL, *Solid Mechanics Module User's Guide* (Stockholm, Sweden, 2021).

[52] See the Supplemental Material at http://link.aps.org/supplemental/10.1103/PhysRevApplied.19.044061 for details of the toy model and the finite-element simulations.

[53] M. P. Makwana and R. V. Craster, Geometrically navigating topological plate modes around gentle and sharp bends, Phys. Rev. B **98**, 184105 (2018).

[54] B. Ash, S. Worsfold, P. Vukusic, and G. Nash, A highly attenuating and frequency tailorable annular hole phononic crystal for surface acoustic waves, Nat. Commun. **8**, 1 (2017).

[55] E. J. Danicki, in *Photonic Band Gaps and Localization* (Springer, 1993), p. 499.

[56] A. Smirnov, B. Zaitsev, I. Nedospasov, G. Nazarov, and I. Kuznetsova, Backward acoustic waves in piezoelectric plates: Possible application as base for liquid sensors, Sensors **23**, 648 (2023).

[57] P. Delsing, A. N. Cleland, M. J. Schuetz, J. Knörzer, G. Giedke, J. I. Cirac, K. Srinivasan, M. Wu, K. C. Balram, and C. Bäuerle, *et al.*, The 2019 surface acoustic waves roadmap, J. Phys. D: Appl. Phys. **52**, 353001 (2019).

[58] J. M. De Ponti, A. Colombi, R. Ardito, F. Braghin, A. Corigliano, and R. V. Craster, Graded elastic metasurface for enhanced energy harvesting, New J. Phys. **22**, 013013 (2020).

[59] J. M. De Ponti, A. Colombi, E. Riva, R. Ardito, F. Braghin, A. Corigliano, and R. V. Craster, Experimental investigation of amplification, via a mechanical delay-line, in a rainbow-based metamaterial for energy harvesting, Appl. Phys. Lett. **117**, 143902 (2020).

[60] J. M. De Ponti, L. Iorio, E. Riva, F. Braghin, A. Corigliano, and R. Ardito, Enhanced energy harvesting of flexural waves in elastic beams by bending mode of graded resonators, Front. Mater. **8**, (2021).

[61] https://doi.org/10.24378/exe.4564.

[62] https://www.meccanospares.com.